# Ozone Sensitivity Analysis and FNR Threshold Division in Beijing Tianjin Hebei Region Based on TROPOMI Data

Hanyang Song , Wenji Zhao * , Xingchuan Yang , Wenxing Hou , Linhan Chen , Pengfei Ma *

Posted Date: 20 September 2023

doi: 10.20944/preprints202309.1284.v1

Keywords: Ozone formation regime; Spatio-temporal change; TROPOMI; BTH

*Article*

# Ozone Sensitivity Analysis and FNR Threshold Division in Beijing Tianjin Hebei Region Based on TROPOMI Data

**Hanyang Song [1], Wenji Zhao [1,*], Xingchuan Yang [1], Wenxing Hou [1], Linhan Chen [2] and Pengfei Ma [2*]**

[1] College of Resource Environment and Tourism, Capital Normal University, Beijing 100048, China; 2210902063@cnu.edu.cn (H.S.); mxoyxc@163.com (X.Y.); gishwx@126.com (W.H.)
[2] Satellite Application Center for Ecology and Environment, MEE, Beijing 100048, China; 15736723276@163.com
* Correspondence: zhwenji1215@163.com (W.Z.); mpf136@163.com (P.M)

**Abstract:** In recent years, the concentration of fine particulate matter ($PM_{2.5}$) in China has decreased significantly, whereas the concentration of surface ozone ($O_3$) has increased. The formation regime of ozone is closely related to the ratio of volatile organic compounds (VOCs) to nitrogen oxides (NOx). To reveal the reasons for this increase in ozone, we determined the sensitivity of ozone generation by determining the regional threshold of the ratio of formaldehyde to nitrogen dioxide ($HCHO/NO_2$) in the satellite troposphere. The different FNR($HCHO/NO_2$) ratio ranges indicate three formation regimes: VOC-limited, transitional, and NOx-limited. The range of the transitional regime plays a crucial role in identifying the regime of ozone formation. Currently, the key threshold for ozone generation in China remains unclear. Polynomial fitting models were used to determine the threshold range for the transitional regime in the BTH region [2.0,3.1]. The ozone formation regime in the BTH region mainly exhibited a transitional and NOx-limited regime, and the overall concentration changes of the HCHO and $NO_2$ columns in the BTH region showed a fluctuating trend from 2019 to 2022. However, compared to 2019, the ozone precursors and FNR showed varying degrees of decline in 2022. The concentration changes of $NO_2$ were high in winter and low in summer, whereas the trend of HCHO and FNR changes was the opposite to that of $NO_2$, being high in summer and low in winter. The concentrations of HCHO and $NO_2$ in the BTH region showed a trend of urban agglomeration areas>urban expansion areas>non-urban areas in different land types from 2019 to 2022, whereas the FNR showed an opposite trend in urban agglomeration areas<urban expansion areas<non-urban areas.

**Keywords:** ozone formation regime; Spatio-temporal change; TROPOMI; BTH

## 1. Introduction

In recent years, with the continuous development of the economy and society, the increasing use of energy, the continuous growth of human activities, and the consumption of large amounts of fossil fuels, environmental air quality has significantly deteriorated, and there have been several air pollution incidents. Since 2013, the Chinese government has implemented several governance plans, however, under these measures, $PM_{2.5}$ has been significantly controlled, while ozone has increased. Various provinces and cities have also adopted strong measures, with atmospheric particulate matter and most gaseous pollutants continuously decreasing nationwide; however, the ozone concentration remains high. Ozone pollution incidents are frequent, and ozone is gradually replacing $PM_{2.5}$ as the primary pollutant [1].

Ozone is an important trace gas in the atmosphere, with stratospheric ozone accounting for approximately 90 % and tropospheric ozone approximately 10 % [2]. They play a crucial role in protecting life through the absorption of harmful ultraviolet rays from the sun. However, surface ozone may pose a threat to human health and the environment. It is formed from the reaction of emissions from cars, factories, and other sources with sunlight. Exposure to high levels of surface ozone can cause a range of health problems, including coughing, throat irritation, chest pain, and shortness of breath. It can also exacerbate asthma and other respiratory diseases, making it difficult for people to breathe [3–6].

 doi:10.20944/preprints202309.1284.v1



Ozone pollution mainly occurs in urban areas with developed industrial transportation and dense populations [7]. When the precursor of ozone is sufficient, meteorological conditions exacerbate ozone pollution, exhibiting regional characteristics. In addition, the relationship between ozone generation and its precursors, such as VOCs and NOx, is nonlinear. Controlling the emission of a single precursor may not effectively reduce ozone concentration, and some regions it may have the opposite effect, leading to an increase in $O_3$ concentration instead of a decrease [8,9]. The sensitivity of ozone generation to NOx and VOCs varies in different environments. According to different sensitivities, the ozone generation control zone can be divided into VOC-limited, NOx-limited, and transitional regimes. If ozone generation in a certain area is in the NOx-limited regime, this indicates that changes in the NOx concentration have the greatest impact on ozone generation. Conversely, in the VOC-limited regime, the control of ozone concentration is mainly based on VOCs. In the transitional regime, reducing any precursor can reduce the ozone concentration [10]. HCHO is a short-term oxidation product of many volatile organic compounds (VOCs), and atmospheric HCHO is an intermediate product of the oxidation of almost all volatile organic compounds (VOCs). It can therefore indicate the overall level of VOCs and can be measured by satellite; due to the short lifespan of NOx and the high proportion of $NO_2$/NOx in the boundary layer, NOx can be approximated by satellite observations of the $NO_2$ column concentration [11].

The transition range of HCHO/$NO_2$ from VOC-limited to NOx-limited regimes varies significantly across different regions of China; VOCs are limited to large urban agglomerations and concentrated in developed cities, and NOx-limited regimes dominate the rest [12–14]. The key threshold for the ozone formation regime in China is currently unclear [15,16], and most existing studies on ozone generation sensitivity based on satellite data have used the ozone generation sensitivity indicator FNR(HCHO/$NO_2$) threshold classification standard established by Duncan et al. in 2010. Thus, [1.0, 2.0] is divided into transitional regimes [10]. The threshold classification criteria for the ozone generation sensitivity index (FNR) were based on model simulations in the US environmental context. However, the actual situation is that there are differences in factors such as ozone precursor emissions, meteorological conditions, and terrain in different regions; therefore, the threshold classification criteria for FNR have regional differences. This means that we need to reassess and adjust the threshold classification criteria based on the characteristics of different regions, to grasp the regime of ozone formation more accurately. Such customized strategies will help to develop more effective VOCs and NOx reduction strategies to address ozone pollution issues in different regions [17].

To effectively control ozone pollution, it is necessary to accurately understand the regime of ozone formation, particularly the spatiotemporal variability of key thresholds for volatile organic compounds (VOCs) and nitrogen oxides (NOx), in key areas of China. Based on this understanding, more effective VOCs and NOx reduction strategies should be developed for different ozone formation regimes, to provide reference opinions on ozone governance in the BTH region.

## 2. Materials and Methods

### *2.1. Study Area*

The Beijing Tianjin Hebei region (BTH) (113° 27–119° 50 E, 36°05–42°40 N) is located in the North China Plain. It is China's "capital economic circle", including 13 cities, namely Beijing (BJ), Tianjin (TJ), Baoding (BD), Tangshan (TS), Langfang (LF), Shijiazhuang (SJZ), Handan (HD), Qinhuangdao (QHD), Zhangjiakou (ZJK), Chengde (CD), Cangzhou (CZ), Xingtai(XT), Hengshui(HS). The gross domestic product of the BTH region in 2022 is 10.0 trillion yuan [18]. The BTH region is the largest and most dynamic economic region in northern China and one of the areas with the densest transportation and logistics networks. The BTH region is an important economic growth pole and driving force for China, with a flat terrain, complex climatic conditions, humid and hot summers, and a strong atmospheric stable layer, which is conducive to the formation and accumulation of ozone [19]. Industrial development and transportation in the region are intensive, and high-emission industries, such as steel, oil refining, the chemical industry, and coal, including coal-fired and motor

Preprints (www.preprints.org) | NOT PEER-REVIEWED | Posted: 20 September 2023 doi:10.20944/preprints202309.1284.v1



vehicle exhaust emissions, have become the main precursors of ozone [20]. In recent years, ozone concentration has shown an annual increasing trend [21,22] and has a clear seasonal variation trend [23]. The average concentration of all national control points in a city is considered to be the average level of ozone in that city, and observation data can be directly used with a high degree of reliability. There is no need to rely on emission inventories to reduce the uncertainty they bring, but as the current distribution of stations is relatively small this leads to monitoring data lacking sufficient detail in certain areas, which limits our comprehensive understanding of the overall distribution of ozone sensitivity in large urban agglomerations. We can use remote sensing data to fill the gap between monitoring stations and to provide continuous coverage. Although research methods based on satellite remote sensing data may be limited by satellite transit time and the uncertainty of the satellite data inversion itself, they have various advantages, such as wide coverage, continuous observation, low cost, constant optimization, and improved spatial resolution [24]. Therefore, studying the sensitivity of ozone generation based on satellite remote sensing data is considered an ideal research method that can help solve the problem of insufficient understanding of the overall distribution of ozone sensitivity in large urban agglomerations.

We used machine and deep learning methods to obtain ozone profiles in the middle and lower tropospheres, by inputting satellite observational data. We obtained surface ozone data, comprehensively evaluated the latest trends in ozone concentrations, and compared the HCHO and $NO_2$ column concentrations provided by TROPOMI with those of ozone precursors. By matching satellite-based HCHO/$NO_2$ measurements with near-surface $O_3$ measurements in various cities in Beijing, Tianjin, and Hebei, we obtained the threshold for the formation and transformation of labeled $O_3$, used it to identify sensitivity indicators for ozone generation and evaluate the regime of ozone formation.

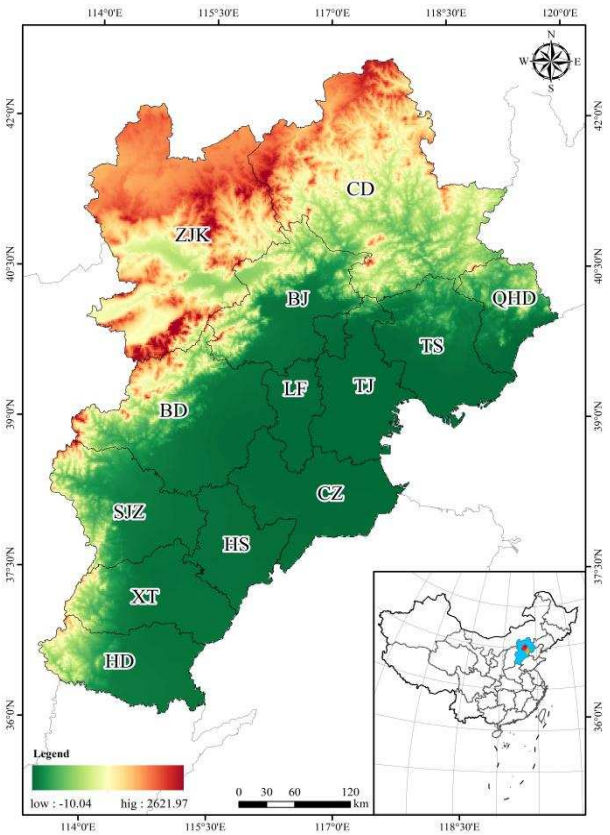


**Figure 1.** Location of the study area with topographical information.

*2.2. Data Sources*

2.2.1. TROPOMI HCHO/$NO_2$

The Tropospheric Monitoring Instrument (TROPOMI) is an instrument used for atmospheric composition observations carried out on the Copernicus Sentinel-5 Precursor (S5P) satellite. This instrument can effectively observe trace gas components in the atmosphere worldwide, including indicators related to human activities, such as $NO_2$, $O_3$, $SO_2$, HCHO, $CH_4$, and CO, and strengthen the observation of aerosols and clouds. TROOMI imaging has a width of 2600 km and covers various parts of the world daily. It has a transit time of 13:30 and the imaging resolution was 7 km×3.5 km. It can more accurately monitor various atmospheric pollutants with significant improvements compared to previous atmospheric composition monitoring remote sensing instruments such as the Moderate-resolution Imaging Spectroradiometer (MODIS), Ozone Monitoring Instrument (OMI), Ozone Mapping and Profiler Suite (OMPS), and Atmospheric Composition Analysis Spectrometer (SCHIMACHY) [25–27]. This study used TROPOMI's HCHO and $NO_2$ column concentration datasets and calculated HCHO/$NO_2$ to study the spatiotemporal changes in HCHO, $NO_2$, and HCHO/$NO_2$ in the BTH region.

The TROOMI Level 2 data products come from three different data streams: near real-time (NRTI), non-time critical or offline (OFFL), and reprocessing (RPRO). NRTI data are available within 3 h of data collection and are suitable for users who need quick access to data and rapid operational processing. However, NRTI data may sometimes be incomplete and have slightly lower data quality than other data streams. Most data users should use offline data available within a few days of collection or the latest version of the reprocessed data. For long-term trend analysis, the latest version of the reprocessed data should be used to avoid changes caused by data version updates. This study used OFFL data with higher data quality and a larger sample size to achieve higher accuracy.

Daily $NO_2$ and HCHO column concentration data were selected for the L2 levels in 2019 and 2022. The storage method for the TROOMI raw data is in netCF4 format, using Python to write scripts, download batches, convert to raster files, perform concatenation, cropping, resampling, and remove outliers. Finally, the daily data were combined into a monthly dataset to calculate the monthly and annual mean concentrations of the $NO_2$ and HCHO columns. TROOMI L2 raw data unit is mol/$m^2$

2.2.2. Surface Ozone Data

The ozone concentration information from ground stations does not accurately reflect the overall ozone concentration in the troposphere. Satellite observation is an effective supplementary method for ground observations that can provide long-term and high-coverage spatial distribution and change information on ozone and its precursors in the troposphere. The China High Air Pollutants (CHAP) dataset was used for near-ground ozone concentrations from 2019 to 2020, which considers the spatiotemporal heterogeneity of air pollution and is generated from big data using artificial intelligence, such as ground measurement, remote sensing products, atmospheric reanalysis, and model simulation.

The surface ozone concentrations in 2021 and 2022 were based on a combination of machine and deep learning. Using this method, we trained the inversion model using the training samples. Based on a well-trained inversion model, near-ground ozone concentration information for the corresponding region can be obtained by inputting satellite observation data to obtain the ozone profile in the middle and lower troposphere.

The inversion technique route, as illustrated in Figure 2, outlines the overall research approach as follows. Firstly, for ultraviolet hyperspectral data, an integrated application study of the LBLRTM and VLIDORT radiative transfer models is conducted. This involves a detailed simulation and analysis within the ultraviolet spectral range, focusing on factors such as aerosols, ring effects, cloud parameters, and ultraviolet polarized light. This study aimed to understand the sensitivity of ozone profile retrieval and error constraint methods to these uncertain factors. It also examines the uncertainty of the a priori covariance matrix, instability mechanisms, and constraint strategies of the inversion model. Within the framework of the optimal estimation method, simultaneous iterative

Preprints (www.preprints.org) | NOT PEER-REVIEWED | Posted: 20 September 2023 doi:10.20944/preprints202309.1284.v1



inversion of tropospheric ozone profiles is performed. Secondly, in conjunction with tropospheric ozone profiles, a Wide&Deep combination model is utilized to analyze multiple parameters affecting near-surface ozone concentrations. This includes the development of an inversion model to obtain high-precision surface ozone concentrations.

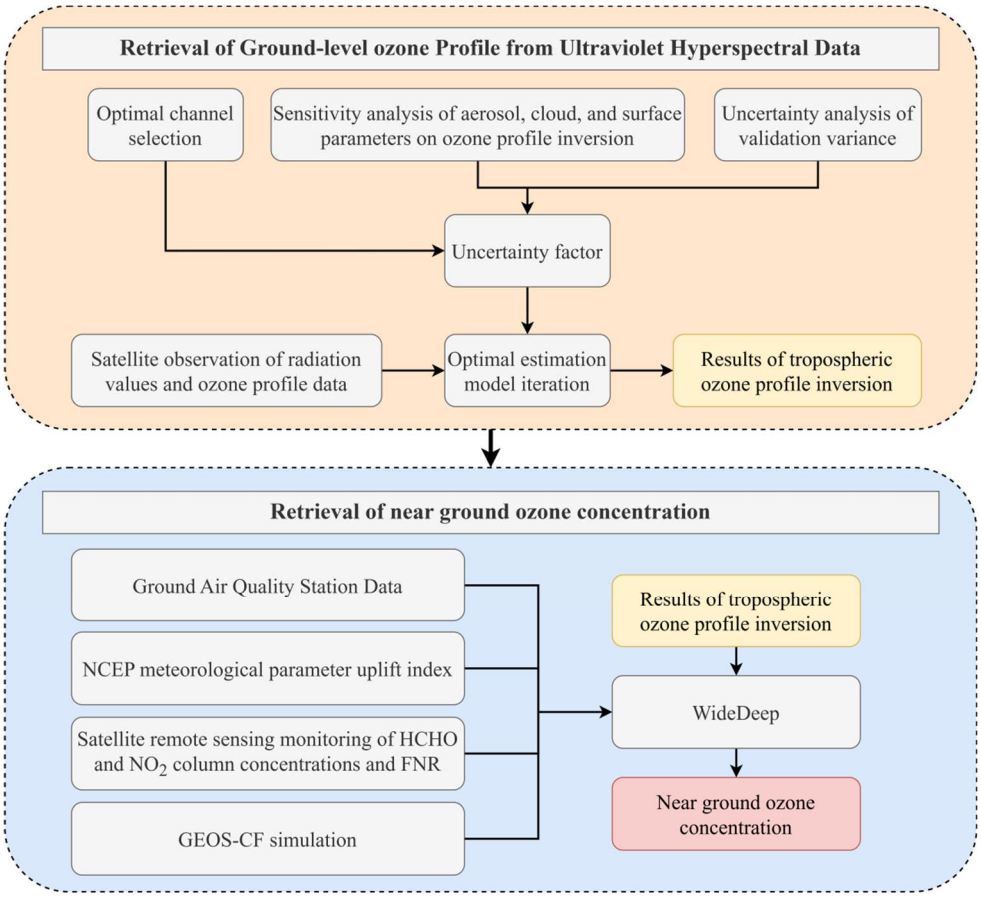


**Figure 2.** Flow chart of near ground ozone concentration inversion.

2.2.3. CLCD Land Cover Product

To compare the differences in ozone formation regimes between cities and rural areas in the BTH region, it was necessary to divide the research area into urban agglomeration, urban expansion, and non-urban areas based on land-cover type products. The current problem is that the resolution of most land cover type products is too low, which has a significant impact on the accuracy of dividing the research area. The China Land Cover Dataset (CLCD) was created by Yang et al. on the Google Earth Engine (GEE) platform, which is the first annual land cover dataset (CLCD) derived from land satellites. A 30 m resolution land cover map of China was established [28]. Figure 3, combined with a comparison of MOODIS (IGBP) products and satellite images, shows that the CLCD has high-resolution and accurate land-cover edges and landscape details. As a 30 m land cover map, CLCD provides accuracy and raw data support for the division of the study area, in order to achieve higher accuracy in the division of the area.

Preprints (www.preprints.org) | NOT PEER-REVIEWED | Posted: 20 September 2023 doi:10.20944/preprints202309.1284.v1



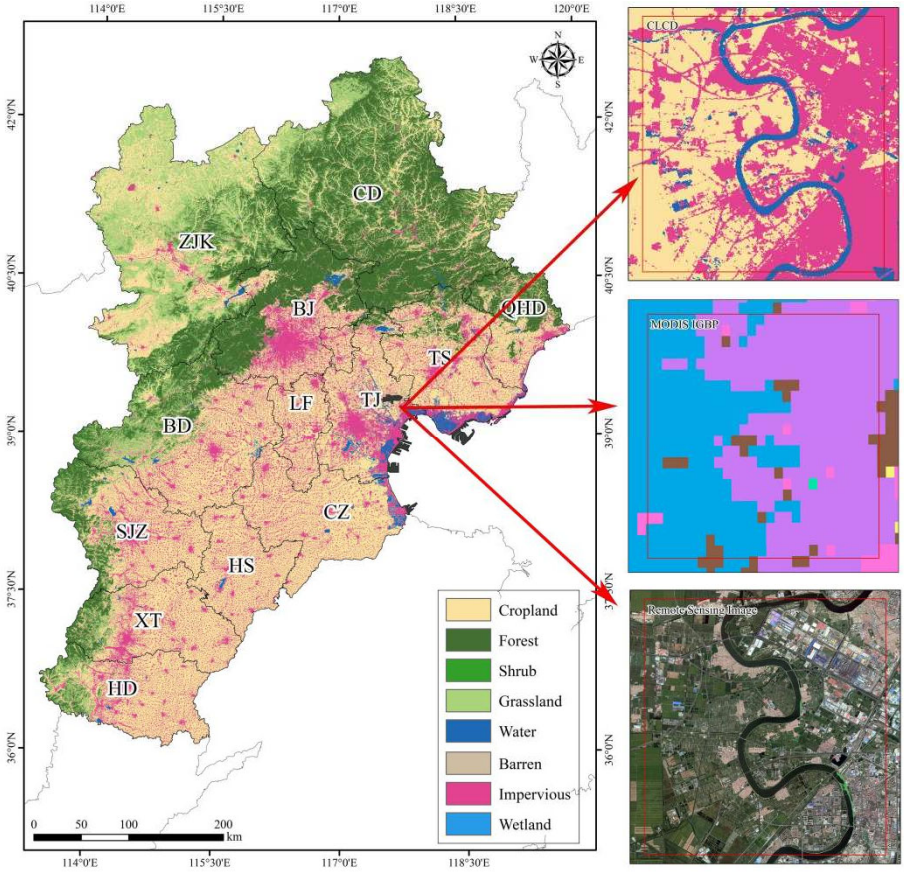


**Figure 3.** Comparison of China land cover dataset, MODIS Land Cover Types, and High-Resolution Remote Sensing Images.

*2.3. Methods*

2.3.1. Comparison of the Ozone Formation Regime between Urban and Non-Urban Areas

To compare the differences in the ozone formation regimes between cities and rural areas in the BTH region, the first and most crucial step was to extract pixels from urban buildings and roads and create a 10 × 10 km grid (totaling 2138) to calculate the proportion of urban and road pixels in the grid area. Areas with an area ratio of more than 50 % were classified as "urban aggregation areas", whereas those with an area ratio of more than 10 % were classified as "urban expansion areas". Areas with an area ratio of less than 10 % were classified as "non-urban areas". Finally, the segmentation results were randomly sampled using remote sensing images with a confidence level of 96 % and confidence interval of 10 %.

2.3.2. Third Order Polynomial Fitting Model

Pusede and Cohen proposed that the ozone excess probability [29] could be used as an effective indicator to study the sensitivity between ozone and its precursors. The specific definition of this indicator is defined as follows: within a certain HCHO/$NO_2$ range, the ratio of the number of days for which ozone exceeds the standard to the total number of days. The formula is as follows:

$$OEP = \frac{Event_{non-attainment}}{Events_{attainment} + Events_{non-attainment}}$$

where $Events_{attainment}$ and $Events_{non\text{-}attainment}$ attachment represent the number of days up to standard and non-standard respectively [29,30].

Preprints (www.preprints.org) | NOT PEER-REVIEWED | Posted: 20 September 2023 doi:10.20944/preprints202309.1284.v1



In this study, a third-order polynomial fitting model was used to fit the nonlinear relationship between HCHO/$NO_2$ and ozone concentrations exceeding the standard rate. Existing studies show that the cubic polynomial fitting model has the highest fitting accuracy and the lowest uncertainty compared to the moving average model and the quadratic polynomial fitting model, and the correlation coefficient (R) of the fitting result is higher than that of the quadratic polynomial fitting model [29]; According to statistics, 391254 pairs of near surface ozone concentration and HCHO/$NO_2$ observation data were used in this study. The vertex of the polynomial fitting curve was considered as the turning point of the transition from VOCs to NOx control. The HCHO/$NO_2$ range corresponding to the first 10 % of the ozone exceedance rate was regarded as the VOCs NOx collaborative control [30].

## 3. Results

### *3.1. Time Trends of Ozone Precursors and FNR*

Figure 4 shows the tropospheric $NO_2$ column concentration, HCHO column concentration, and FNR in the BTH region from 2019 to 2022. According to the fitting results of the time variation trend of the monthly average concentration, the peak value of $NO_2$ was in winter (December 2020, concentration of $18.00\times10^{15}$ mol/cm$^2$), and the concentration was the lowest in summer (August 2022 concentration of $3.70\times10^{15}$ mol/cm$^2$). The trend in HCHO change was opposite to that of $NO_2$, with a peak occurring in summer and the lowest concentration in winter. The peak concentration occurred in June 2019, with a concentration of $18.76\times10^{15}$ mol/cm$^2$, reaching its lowest concentration in April 2021 at $9.20\times10^{15}$ mol/cm$^2$. The trend in the FNR variation was similar to that of HCHO, reaching its peak in summer and its lowest point in winter. The maximum value occurred in July 2019 and the minimum value occurred in January 2021, with values of 4.75 and 1.04, respectively.

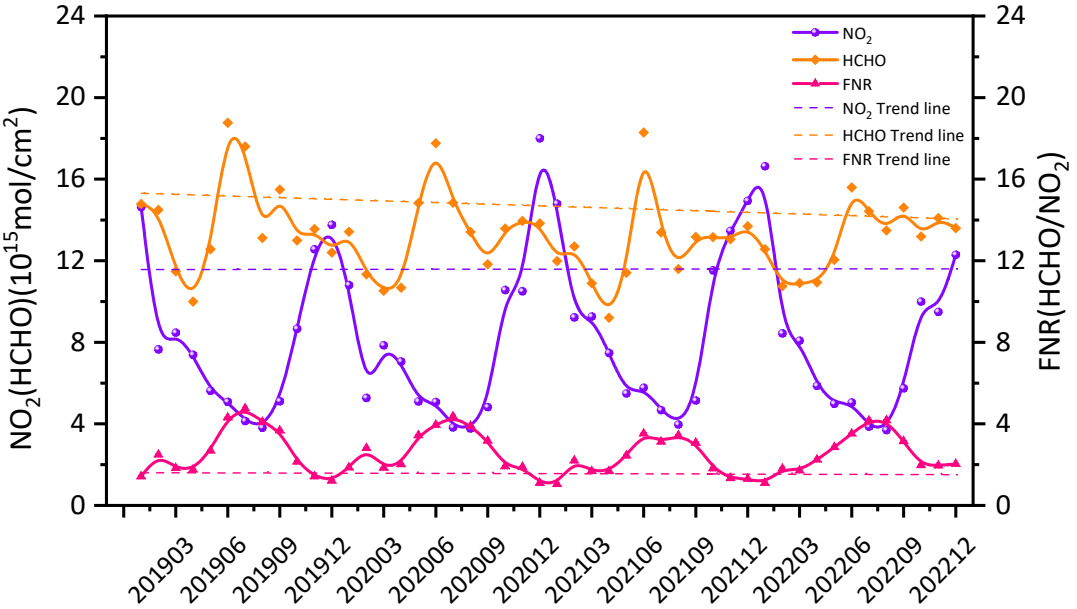


**Figure 4.** 2019-2022 $NO_2$ column concentration, HCHO column concentration, and FNR time variation trend in the BTH region.

### *3.2. Interannual Variations of HCHO and NO2 Column Concentrations under Different Ground Features*

Figure 5 shows the interannual changes in the tropospheric NO2 column concentration, HCHO column concentration, and FNR in the BTH region and their trends in various land use types. During this period, the concentration of the tropospheric $NO_2$ column had no obvious interannual variation trend. The concentration will reach a maximum of $10.19\times10^{15}$ mol/cm$^2$ in 2021 and a minimum of

Preprints (www.preprints.org) | NOT PEER-REVIEWED | Posted: 20 September 2023 doi:10.20944/preprints202309.1284.v1



8.81 × $10^{15}$ mol/cm² in 2020. HCHO showed an interannual trend of first decreasing and then increasing. The highest concentration point appeared in 2019, which was 14.48 × $10^{15}$ mol/cm², and the lowest concentration point was in 2021, which was 13.10 × $10^{15}$ mol/cm². The FNR exhibited the opposite trend to the $NO_2$ column concentration, reaching a peak of 2.40 in 2020 and a minimum of 1.97 in 2021. It is possible that changes in the containment policy of the pandemic may have affected emissions from factories and traffic sources, and the concentrations of HCHO and $NO_2$ showed a fluctuating trend from 2019 to 2022. However, compared with 2019, ozone precursors and FNR showed different degrees of decline in 2022, with $NO_2$ concentration decreasing by approximately 2.8 %, HCHO concentration decreasing by approximately 6.6 %, and FNR decreasing by approximately 3.4 %.

From 2019 to 2022, the concentration changes of $NO_2$ column concentration and HCHO column concentration in different ground features can be seen as urban agglomeration>urban expansion>non-urban areas, and FNR is the opposite trend urban agglomeration<urban expansion<non-urban areas, which can be seen that anthropogenic emissions account for a high proportion of emissions in BTH region. $NO_2$ in urban agglomerations decreased by 0.98 × $10^{15}$ mol/cm², from 11.86 × $10^{15}$ mol/cm² in 2019 to 10.88 × $10^{15}$ mol/cm² in 2022; in the urban expansion area, it decreased from 9.91 × $10^{15}$ mol/cm² to 9.60 × $10^{15}$ mol/cm², a decrease of 0.31 × $10^{15}$ mol/cm²; in non-urban areas, it decreased from 6.40 × $10^{15}$ mol/cm² to 6.22 × $10^{15}$ mol/cm², a decrease of 0.18 × $10^{15}$ mol/cm². HCHO decreased by 1.34 × $10^{15}$ mol/cm² from 15.70 × $10^{15}$ mol/cm² in 2019 to 14.36 × $10^{15}$ mol/cm² in 2022 in urban agglomeration areas, by 1.24 × $10^{15}$ mol/cm² from 14.88 × $10^{15}$ mol/cm² to 13.64 × $10^{15}$ mol/cm² in urban expansion areas, and by 0.55 × $10^{15}$ mol/cm² from 12.84 × $10^{15}$ mol/cm² to 12.29 × $10^{15}$ mol/cm² in non-urban areas; From 2019 to 2022, FNR did not change in urban agglomeration areas, but decreased from 2.04 to 1.89 in urban expansion areas and from 3.36 to 3.31 in non-urban areas. The $NO_2$ and HCHO column concentrations showed the most significant downward trend in urban agglomeration areas and the smallest decline in non-urban areas, indicating that emission reduction policies in cities have played a significant role.

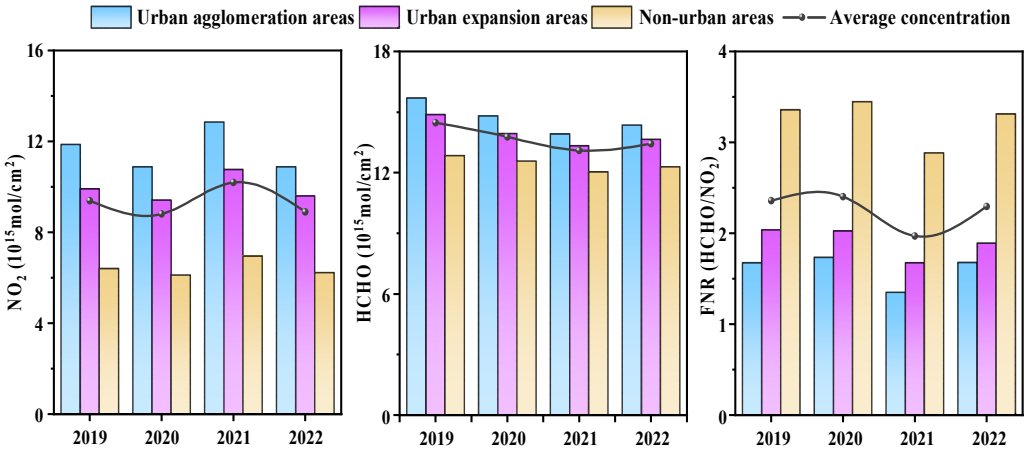


**Figure 5.** 2019-2022 $NO_2$ column concentration, HCHO column concentration, and FNR interannual variation trend of various land use types in the BTH region.

*3.3. Estimation of Transition Range of Ozone Formation Regime in BTH Region*

Owing to the complex nonlinear relationship between near-surface ozone concentration and its precursor concentration, effective control of ozone concentration remains a challenge in the reduction of air pollutant emissions. To determine the key threshold of the overall ozone formation regime in the BTH region, this study divided the FNR (HCHO/$NO_2$) into 2138 equal parts, combined with the near-surface ozone, and calculated the ozone exceeding the standard rate in each equal part in the ozone season (April September). Firstly, a cubic polynomial model was used for nonlinear fitting of the ozone excess rate and HCHO/$NO_2$. The fitting results for the BTH region are shown in Figure 6.

Preprints (www.preprints.org) | NOT PEER-REVIEWED | Posted: 20 September 2023 doi:10.20944/preprints202309.1284.v1



The peak value of the curve is 2.65, and the shadows on both sides are collaborative control areas with a range of [2.0,3.1]

Compared to previous studies, Chen et al. [18] used FNR (OMI HCHO/$NO_2$) and ground monitoring $\Delta O3/\Delta NO_2$, and found that the statistical relationship between $NO_2$ (the ratio of ozone change rate and $NO_2$ change rate between consecutive months) shows that the collaborative control range of the BTH region from 2014 to 2016 is [0.65,1.21], Li et al. [36] used CCM model and polynomial fitting model to get [1.2,2.1], and Ren et al. [38] used EKMA curve and the nonlinear relationship between ozone and FNR (OMI HCHO/$NO_2$) to get that the collaborative control range of BTH region is [2.2,3.2], There are large differences in the range of transitional regimes in local space [39,40]. This situation may be affected by many factors, including the selection of the research period, dataset used, and spatial resolution of the dataset. In some local areas and megalopolises, serious pollution problems may lead to expansion of the transitional regime range [40]. In addition, the uncertainty in the satellite-observed HCHO and $NO_2$ data should be considered, which may negatively affect the estimation results.

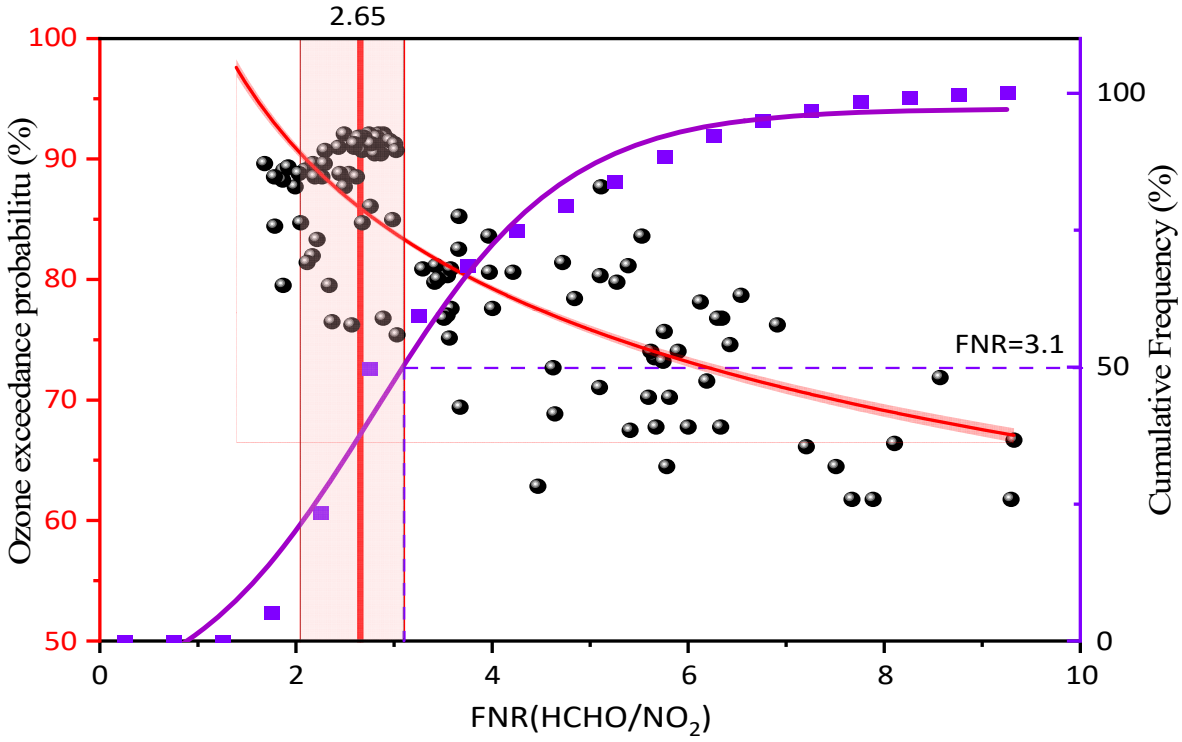


**Figure 6.** Fitting ozone exceedance probability to HCHO/NO2 through the third-order polynomial model.

*3.4. Spatial Distribution of $O_3$ Formation Regimes*

Based on the nonlinear relationship of $O_3$-NOx-VOC, the change in ozone precursors is an important factor affecting ozone levels. Based on the long-time series TROPOMI satellite remote sensing data, this study explored the spatial variation characteristics of HCHO and $NO_2$ column concentrations and surface ozone concentration and FNR in the high incidence season of ozone pollution (April September) in the BTH region from 2019 to 2022, and calculated the spatial distribution map from April to September. It can be seen from Figure 7 that there are significant differences in $NO_2$ column concentrations between cities in the BTH region and surrounding areas. High $NO_2$ column concentrations were mainly concentrated in the central regions of BJ, TJ, TS, and the western regions of SJZ, XT, and HD. This area has a large population, developed industry and transportation, and a large number of motor vehicles, especially in large cities such as BJ and TJ [31,32]. Automobile fuel combustion produces nitrogen oxides (NOx), of which nitrogen dioxide

Preprints (www.preprints.org) | NOT PEER-REVIEWED | Posted: 20 September 2023 doi:10.20944/preprints202309.1284.v1



($NO_2$) is an important component. The pollution of $NO_2$ is not only related to human activities but also has the effect of urban agglomeration, and cities affect each other [33,34].

The spatial variation of the HCHO column concentration in the BTH region was not as significant as that of the $NO_2$, and the difference in the concentration gradient was small. High concentrations in the HCHO column were mainly concentrated in the central and southern areas of the BTH region. The concentrations in CD and ZJK in the north were relatively low. Formaldehyde is mainly formed by the oxidation of volatile organic compounds (VOCs), and its concentration in the atmosphere is affected by VOC emission sources [35]. In contrast, $NO_2$ is mainly related to vehicle exhaust and industrial emissions, and their concentration distribution may be more affected by these sources. The source distribution of formaldehyde may have been more dispersed, leading to a difference in its spatial variation.

The spatial distribution characteristics of the ozone generation sensitivity in the BTH region are shown in Figure 7. CD, ZJK, northern and western BJ, Western BD, and Western SJZ are mainly controlled by NOx. Central BJ, TJ, TS, and HD were mainly controlled by VOCs. LF, HS, CZ, HD, XT, Eastern SJZ, and Eastern BD are under transitional regime control. The VOC-limited regimes showed an overall downward trend, and the transitional and NOx-limited regimes gradually expanded in the BTH region [36].

The spatial distribution of the ozone concentration in the BTH region is high in the southeast and low in the northwest. Southeastern BTH is a region where urbanization and industrialization are relatively concentrated. A large volume of VOCs and NOx emissions in these regions may contribute to the formation of ozone. However, the northwestern region is usually more rural, with less human activity and lower VOCs and NOx emissions, resulting in lower ozone concentrations. The wind direction and meteorological conditions also affected the distribution of ozone. The southeastern region is usually affected by a marine climate, and wind from the ocean may lead to the transport and accumulation of ozone, thus increasing its concentration. However, the meteorological conditions in Northwest China are relatively dry, which may not be conducive to the transmission and accumulation of ozone [22]; therefore, its concentration is low.

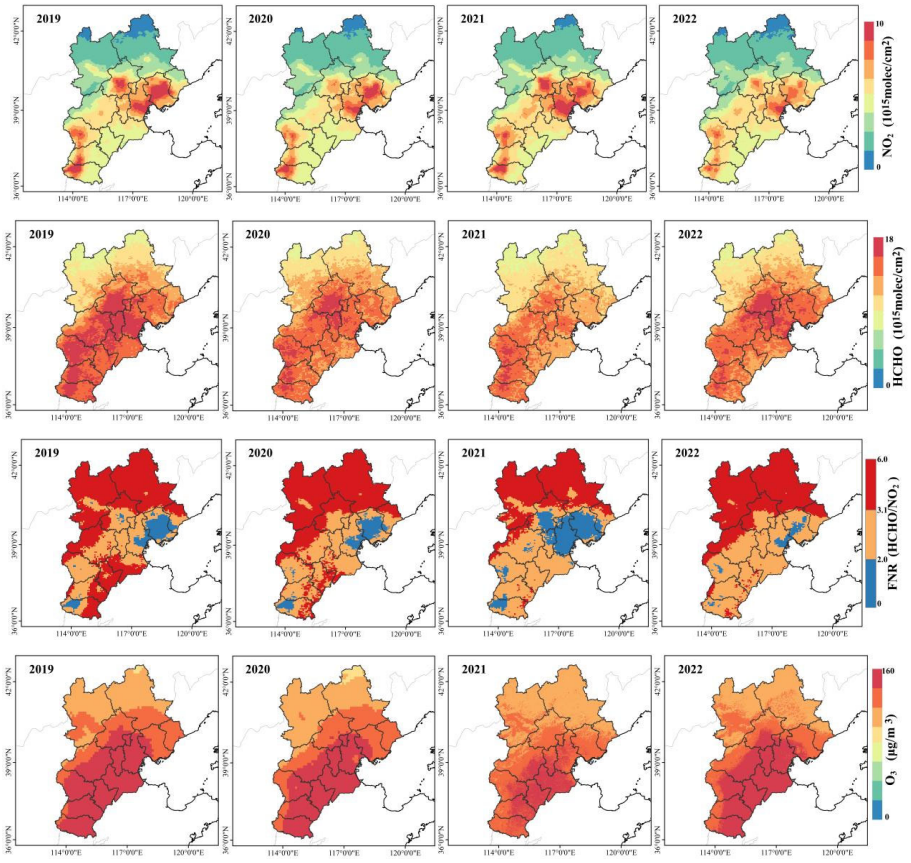

Preprints (www.preprints.org) | NOT PEER-REVIEWED | Posted: 20 September 2023 doi:10.20944/preprints202309.1284.v1



**Figure 7.** Spatial distribution map of $NO_2$, HCHO, FNR, and $O_3$ mean values in the BTH region from April to September 2019-2022.

*3.5. Change in the Ozone Generation Sensitivity Threshold in BTH Region*

Figure 8 shows the change in the ozone generation-sensitive areas of different land cover types in the BTH region during the period of high ozone incidence (April–September) from 2019 to 2022. From the overall change trend of the BTH region, the VOC-limited regimes decreased from 8 % in 2019 to 3.7 % in 2022, the collaborative control area increased from 30.5 % to 42.6 %, and the NOx-limited regimes decreased from 54.3 % to 46.3 %, indicating that the ozone formation regime in the BTH region was mainly transitional and NOx-limited. The change in ozone sensitivity in the BTH area is the most significant in 2021, showing that the proportion of VOC-limited regimes has increased, which is significantly higher than that in other years; the proportion in urban agglomeration areas has reached 71.5 %, which is directly related to the increase in $NO_2$ concentration and the decrease in HCHO concentration in the BTH region in 2021.

From 2019 to 2022, urban agglomeration, urban expansion, and non-urban areas showed an overall trend of decreasing VOC-limited regimes and increasing transitional regimes. The VOC-limited regimes decreased by 10.3 %, 9.8 %, and 3.8 %, respectively, while the transitional regimes increased by 4.6 %, 17.2 %, and 12.7 %, respectively. The urban agglomeration area increased by 5.7 % in the NOx-limited regimes, and the urban expansion area and non-urban area decreased by 7.5 %. These results indicate that VOC-limited regimes are mainly distributed in urban agglomeration areas, transitional regimes are mainly concentrated in urban expansion areas, and non-urban areas are mainly controlled by NOx. This is because there are huge differences in vehicle exhaust emissions, industrial production emissions, domestic emissions, and other aspects between urban and non-urban areas [37]; therefore, the NOx concentration in urban areas is significantly higher than that in non-urban areas, and HCHO/$NO_2$ in the non-urban areas of the BTH region is higher than that in urban areas. NOx emissions reduction in non-urban areas reduces the concentration of ozone more effectively than that in urban areas.

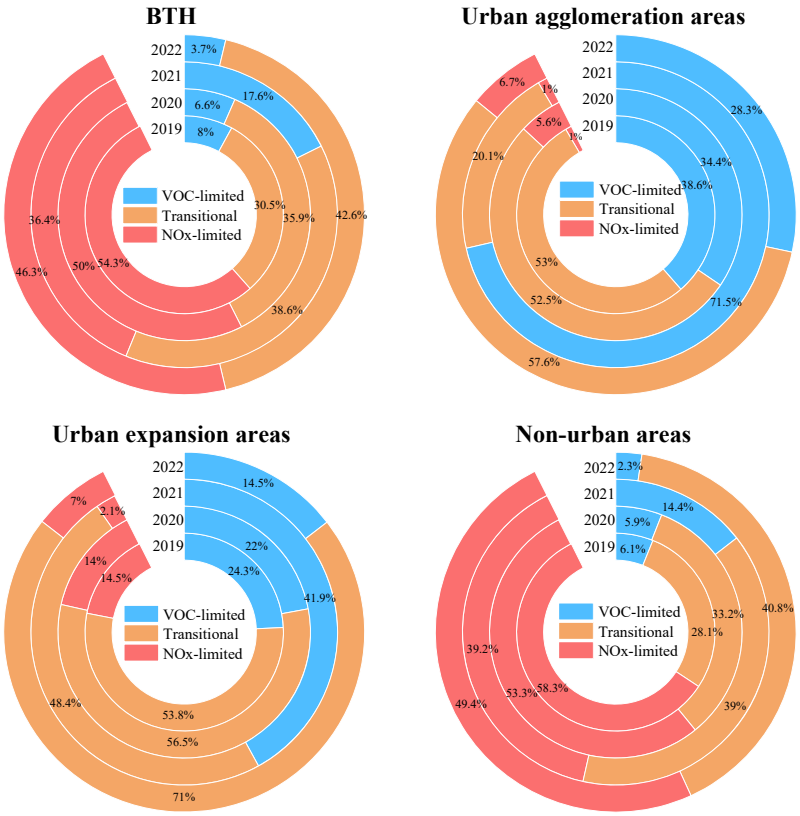

 doi:10.20944/preprints202309.1284.v1



**Figure 8.** Changes in sensitive types of ozone generation under different land cover types in the BTH region from 2019 to 2022.

## 4. Discussion

This study combined TROPOMI HCHO and $NO_2$ satellite observation data with surface ozone concentrations and applied a polynomial fitting model to explore the nonlinear relationship between ozone and its precursors. The VOC-limited regimes decreased in the BTH region, whereas the NOx-limited and transitional regimes showed an expanding trend. The BTH region shows transitional and NOx-limited regimes. However, this study still has some limitations. First, there were some errors in the retrieval process of HCHO and $NO_2$ satellite observation data, which may have impacted the accuracy of the research results. In addition, although the TROPOMI satellite provides high-resolution pollutant data, there is still a lack of long-term series data, which limits in-depth study of long-term trends. Future research should focus on the accuracy and availability of data to improve the comprehensive understanding of air pollution in the BTH region, and propose pollutant emission reduction strategies better suited for this region. Secondly, a single method polynomial fitting model was used to estimate the threshold of the ozone formation regime, and the research conclusion will be the indetermination of a certain degree.

## 5. Conclusions

Based on TROPOMI HCHO and $NO_2$ concentration satellite observation data and near-surface ozone data, this study explored the temporal and spatial variation characteristics of HCHO, $NO_2$, FNR, and ozone concentrations in the BTH region and under different ground features, and preliminarily studied the sensitivity threshold of ozone formation. The main conclusions are as follows.

(1) The concentration of HCHO and $NO_2$ in the column in the BTH region fluctuated between 2019 and 2022. However, compared with 2019, ozone precursors and FNR decreased by different degrees in 2022, with $NO_2$ concentration decreasing by approximately 2.8 %, HCHO concentration decreasing by approximately 6.6 %, and FNR decreasing by approximately 3.4 %. The concentration of $NO_2$ is high in winter and low in summer. The change trends of HCHO and FNR were opposite to those of $NO_2$, being high in summer and low in winter, indicating that different pollution control measures should be taken according to different time periods.

(2) The concentrations of HCHO and $NO_2$ in the BTH region from 2019 to 2022 showed the following trend: urban agglomeration>urban expansion>non-urban areas. FNR showed the opposite trend: urban agglomeration<urban expansion<non-urban areas. The difference in NOx concentrations between different ground types was the main explanation for this phenomenon. The FNR ($HCHO/NO_2$) in non-urban areas was higher, and NOx emission reduction in this region would more effectively reduce the near-surface ozone concentration. In urban areas, there is a trend from VOC control type to VOCs NOx collaborative control type. Controlling the concentrations of VOCs and NOx simultaneously in this area will have a better effect on the treatment of ozone pollution than reducing NOx alone.

(3) The spatial distributions of HCHO, $NO_2$ column concentrations, and near-ground ozone concentrations in the BTH region showed a trend toward high concentrations in the southeast and low concentrations in the northwest. This is because the southeast region has concentrated areas of urbanization and industrialization, a large population, developed transportation, and a large number of motor vehicles.

(4) This study was based on the satellite inversion of near-ground ozone concentration data and ozone precursor concentration data. A cubic polynomial fitting model was used to localize the ozone generation threshold in the BTH region. Preliminary research results show that the range of transitional regimes is [2.0, 3.1], and the ozone formation regime in the BTH region mainly follows transitional and NOx-limited regimes. From the perspective of land cover types, VOC-limited regimes are mainly distributed in urban agglomeration areas, transitional regimes are mainly concentrated in urban expansion areas, and non-urban areas are mainly controlled by NOx.

**Author Contributions:** Conceptualization, H. S.; methodology, P. M.; software, W. H.; validation, W. Z.; formal analysis, H. S.; resources, P. M.; data curation, X. Y. All authors have read and agreed to the published version of the manuscript.

**Funding:** This research was supported by the National Natural Science Foundation of China (Grants 42071422,42305198), and the Beijing Postdoctoral Research Foundation (Grants 2023-ZZ-149).

**Institutional Review Board Statement:** Not applicable.

**Informed Consent Statement:** Not applicable.

**Data Availability Statement:** Not applicable.

**Acknowledgments:** We thank Wenxing Hou for contributing to the design of the data analysis framework.

**Conflicts of Interest:** The authors declare no conflicts of interest.

## References

1. Zhang, Q.; Zhao, Y.X.; Tong, D.; Shao, M.; Wang, S.X.; Zhang, Y.H.; Xu, X.D.; Wang, J.N.; He, Hong.; Liu, W.Q.; et al. Drivers of improved $PM_{2.5}$ air quality in China from 2013 to 2017. *Proc Natl Acad Sci U S A* **2019**, *116*.
2. Chen, L.J. *A Study on the Evolution of Ozone Pollution in China and Regional Management Methods [D]*; China University of Geosciences: Beijing (Beijing), 2018.
3. Aneja, V.P.; Li, Z. Characterization of ozone at high elevation in the eastern United States: Trends,seasonal variations, and exposure. *J Geophys Res* **1992**, *97*, 9873–9888. DOI:10.1029/92JD00503.
4. Linn, W.S.; Shamoo, D.A.; Anderson, K.R.; Peng, R.C.; Avol, E.L.; Hackney, J.D. Effects of prolonged, repeated exposure to ozone, sulfuric acid, and their combination in healthy and asthmatic volunteers. *Am J Respir Crit Care Med* **1994**, *150*, 431–440. DOI:10.1164/ajrccm.150.2.8049826.
5. Xie, Y.; Dai, H.; Zhang, Y.; Wu, Y.; Hanaoka, T.; Masui, T. Comparison of health and economic impacts of PM2.5 and ozone pollution in China. *Environ Int* **2019**, *130*, 104881. DOI:10.1016/j.envint.2019.05.075.
6. Liu, H.; Liu, S.; Xue, B.; Lv, Z.; Meng, Z.; Yang, X.; Xue, T.; Yu, Q.; He, K. Ground-level ozone pollution and its health impacts in China. *Atmos Environ* **2018**, *173*, 223–230. DOI:10.1016/j.atmosenv.2017.11.014.
7. Wang, X.S.; Li, J.L.; Zhang, Y.H.; Xie, S.D.;. Tang, X.Y.;. Ozone source attribution during a severe photochemical smog episode in Beijing, China. *Sci Sin* (Chimica) **2009**, *39*, 548–559.
8. Zhang, Y.H.; Su, H.; Zhong, L.J.; Cheng, Y.F.; Zeng, L.M.; Wang, X.S.; Xiang, Y.R.; Wang, J.L.; Gao, D.F.; Shao, M. Regional ozone pollution and observation-based approach for analyzing ozone-precursor relationship during the PRIDE-PRD2004 campaign ［J］. *Atmos Environ* **2008**, *42*, 6203–6218. DOI:10.1016/j.atmosenv.2008.05.002.
9. Huang, C.; Chen, C.H.; Li, L.; Cheng, Z.; Wang, H.L.; Huang, H.Y.; Streets, D.G.; Wang, Y.J.; Zhang, G.F.; Chen, Y.R. Emission inventory of anthropogenic air pollutants and VOC species in the Yangtze River Delta region, China［J］. *Atmos Chem Phys* **2011**, *11*, 4105–4120. DOI:10.5194/acp-11-4105-2011.
10. Duncan, B.N.; Yoshida, Y.; Olson, J.R.; Sillman, S.; Martin, R.V.; Lamsal, L.; Hu, Y.; Pickering, K.E.; Retscher, C.; Allen, D.J.; et al. Application of OMI observations to a space-based indicator of NOx and VOC controls on surface ozone formation. *Atmos Environ* **2010**, *44*, 2213–2223. DOI:10.1016/j.atmosenv.2010.03.010.
11. Chan, K.L.; Wang, Z.R.; Ding, A.J.; Heue, K.P.; Shen, Y.C.; Wang, J.; Zhang, F.; Shi, Y.N.; Hao, N.; Wenig, M. MAX-DOAS measurements of tropospheric $NO_2$ and HCHO in Nanjing and a comparison to ozone monitoring instrument observations. *Atmos Chem Phys* **2019**, *19*, 10051–10071. DOI:10.5194/acp-19-10051-2019.
12. Lu, K.D.; Zhang, Y.H.; Su, H.; Zhao, Shao.M.; Zeng, L.M.; Zhong, L.J.; Xiang, Y.R.; Chang, C.C. Chou, C.K.; Andreas, W. . Regional ozone pollution and key controlling factors of photochemical ozone production in Pearl River Delta during summer time. Scientia Sinica: Chimica **2010**, *40*, 407–420.
13. Zhuang, L.Y.; Chen, Y.P.; Fan, L.Y.; Ye, D.Q. Study on the ozone formation sensitivity in the Pearl River Delta based on OMI satellite data and MODIS land cover type products. *Acta Sci Circum* **2019**, *39*, 3581–3592.
14. Zhuang, L.Y. *Ground Level Ozone Concentration Characteristics and Formation Sensitivity in China's Three Agglomerations [D]*; South China University of Technology: Guangzhou, 2019.
15. Wei, W.; Li, Y.; Ren, Y.; Cheng, S.; Han, L. Sensitivity of summer ozone to precursor emission change over Beijing during 2010–2015: A WRF-Chem modeling study. *Atmos Environ* **2019**, *218*, (116984). DOI:10.1016/j.atmosenv.2019.116984.

16. Wang, P.; Chen, Y.; Hu, J.; Zhang, H.; Ying, Q. Attribution of tropospheric ozone to NOx and VOC emissions: Considering ozone formation in the transition regime. *Environ Sci Technol* **2019**, *53*, 1404–1412. DOI:10.1021/acs.est.8b05981.
17. Cheng, L.J.; Wang, S.A.; Gong, Z.Y.; Li, H.; Yang, Q. Spatial and seasonal variation and regionalization of ozone concentrations in China. *China Environ Sci* **2017**, *37*, 4003–4012.
18. Available online: https://data.stats.gov.cn/easyquery.htm?cn=E0103&zb=A0202&reg=110000&sj=2022.
19. Hu, L.M.; Li, Y.X.; Shi, N.F.; S, Y.;. Spatiotemporal change characteristics of ozone concentration in Beijing-Tianjin-Hebei region. *Environ Sci Technol* **2019**, *42*, 1–7.
20. Yan, H.; Zhang, W.; Hou, M.; Li, Y.S.; Gao, P.; Xia, Q. Meng, X.Y.; Fan, L.Y.; Ye, D.Q. Sources and control area division of ozone pollution in cities at prefacture level and above in China. *Environ Sci* **2020**, *41*, 5215–5224.
21. Wang, M.; Zheng, Y.F.; Liu, Y.J.; Li, Q.P.; Ding, Y.H. Characteristics of ozone and its relationship with meteorological factors in Beijing-Tianjin-Hebei Region. *China Environ Sci* **2019**, *39*, 2689–2698.
22. Yu, Y.J.; Meng, X.Y.; Wang, Z.; Zhou, W.; Yu, H.X. Driving factors of the significant increase in surface ozone in the Beijing-Tianjin-Hebei region, China, during 2013~2018. *Huan Jing Ke Xue* **2020**, *41*, 106–114. DOI:10.13227/j.hjkx.201905222.
23. Yao, Q.; Ma, Z.Q.; Hao, T.Y.; Fan W.Y.; Yang, X; Tang, Y.X.; Cai, Z.Y.; Han, S.Q. Temporal and spatial distribution characteristics and background concentration estimation of ozone in Beijing-Tianjin-Hebei region. *China Environ Sci* **2021**, *41*, 4999–5008.
24. *Spatial and Temporal Distribution Characteristics, Simulation and Observation Research of HCHO and NO in China*.
25. Zhu, L. *Satellite Data to Freshman*. Available online: http://www.satdatafresh.com, 2022, total ozone column daily Product.
26. Available online: https://sentinel.esa.int/web/sentinel/missions/sentinel-5p.
27. Available online: https://sentinel.esa.int/web/sentinel/user-guides/sentinel-5p-tropomi.
28. Yang, J.; Huang, X. The 30 m annual land cover dataset and its dynamics in China from 1990 to 2019. *Earth Syst Sci Data* **2021**, *13*, 3907–3925. DOI:10.5194/essd-13-3907-2021.
29. Pusede, S.E.; Cohen, R.C. On the observed response of ozone to NOx and VOC reactivity reductions in San Joaquin valley California 1995-present. *Atmos Chem Phys* **2012**, *12*, 8323–8339. DOI:10.5194/acp-12-8323-2012.
30. Jin, X.; Fiore, A.; Boersma, K.F.; Smedt, I.; Valin, L. Inferring changes in summertime surface ozone-NOx-VOC chemistry over U.S. urban areas from two decades of satellite and ground-based observations. *Environ Sci Technol* **2020**, 54, 6518–6529. DOI:10.1021/acs.est.9b07785.
31. Wei, J.; Li, Z.; Li, K.; Dickerson, R.R.; Pinker, R.T.; Wang, J.; Liu, X.; Sun, L.; Xue, W.; Cribb, M. Full-coverage mapping and spatiotemporal variations of ground-level ozone ($O_3$) pollution from 2013 to 2020 across China. *Remote Sens Environ* **2022**, 270, 112775. DOI:10.1016/j.rse.2021.112775.
32. Zheng, X.X.; Li, L.J.; Zhao, W.J.; Zhao, W.H. Spatial and temporal characteristics of atmospheric $NO_2$ in the Beijing Tianjin-Hebei region. *Ecol Environ Sciences* **2014**, *23*, 1938–1945.
33. Crutzen, P.J. The role of NO and $NO_2$ in the chemistry of the troposphere and stratosphere. *Annu Rev Earth Planet Sci* **1979**, *7*, 443–472. DOI:10.1146/annurev.ea.07.050179.002303.
34. Liu, X.T.; Zheng, T.F.; Wan Q.L.; Tan, H.B.; Deng, X.J.; Fei, L.I.; Deng, T. Spatiotemporal characteristics of $NO_2$ in concentrated PRD urban districts and analysis of anthropogenic influences based on OMI remote sensing data[J]. *J Trop Meteorology* **2015**, *31*, 193–201.
35. Zhu, S.; Li, X.; Yu, C.; Wang, H.; Wang, Y.; Miao, J. Spatiotemporal variations in satellite based formaldehyde (HCHO) in the Beijing-Tianjin-Hebei region in China from 2005 to 2015. *Atmosphere* **2018**, *9*, 5. DOI:10.3390/atmos9010005.
36. Li, Ruiyuan; Xu, Miaoqing; Li, M.; Chen, Z.; Gao, Bingbo; Zhao, N.; Yao, Q. Identifying the spatiotemporal variations of ozone formation regimes across China from 2005 to 2019 based on polynomial simulation and causality analysis. *Atmos Chem Phys Discuss* **2021**, 1–28.
37. Cheng, N.; Li, R.; Xu, C.; Chen, Z.; Chen, D.; Meng, F.; Cheng, B.; Ma, Z.; Zhuang, Y.; He, B.; et al. Ground ozone variations at an urban and a rural station in Beijing from 2006 to 2017: Trend, meteorological influences and formation regimes. *J Clean Prod* **2019**, *235*, (11–20). DOI:10.1016/j.jclepro.2019.06.204.
38. Ren, J.; Guo, F.; Xie, S. Diagnosing ozone–NO x –VOC sensitivity and revealing causes of ozone increases in China based on 2013–2021 satellite retrievals. *Atmos Chem Phys* **2022**, *22*, 15035–15047. DOI:10.5194/acp-22-15035-2022.
39. Schroeder, J.R.; Crawford, J.H.; Fried, A.; Walega, J.; Weinheimer, A.; Wisthaler, A.; Müller, M.; Mikoviny, T.; Chen, G.; Shook, M.; et al. New insights into the column $CH_2O/NO_2$ ratio as an indicator of near-surface ozone sensitivity. *J Geophys Res Atmos* **2017**, *122*, 8885–8907. DOI:10.1002/2017JD026781.

40. Jin, X.; Fiore, A.M.; Murray, L.T.; Valin, L.C.; Lamsal, L.N.; Duncan, B.; Boersma, K.F.; De Smedt, I.; Abad, G.G.; Chance, K.; et al. Evaluating a space-based indicator of surface ozone-NOxVOC sensitivity over midlatitude source regions and application to decadal trends. *J Geophys Res Atmos* **2017**, *122*, 10–461. DOI:10.1002/2017JD026720.